Prediction of the Spectrum of a Digital Delta–Sigma Modulator Followed by a Polynomial Nonlinearity

Kaveh Hosseini, *Member, IEEE*, Michael Peter Kennedy, *Fellow, IEEE*, Stephen H. Lewis, *Fellow, IEEE*, and Bernard C. Levy, *Fellow, IEEE*

***Abstract*—This paper presents a mathematical analysis of the power spectral density of the output of a nonlinear block driven by a digital delta–sigma modulator. The nonlinearity is a memoryless third-order polynomial with real coefficients. The analysis yields expressions that predict the noise floor caused by the nonlinearity when the input is constant.**

***Index Terms*—Digital-to-analog converters, fractional-N frequency synthesizer, digital delta–sigma modulator (DDSM).**

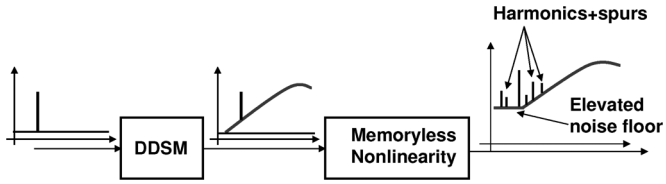

Fig. 1. DDSM, followed by a memoryless nonlinearity. The spectrum of the DDSM's output is distorted after it is applied to the nonlinearity.

I. Introduction

THE focus of research into improving the spectral performance of digital delta–sigma modulators (DDSMs) has been on ensuring that their output spectra do not contain undesirable (spurious) tones resulting from insufficient randomization and/or short cycles [1]–[17]. One normally assumes that the quantizer error introduced in a DDSM is white and independent of the input signal. If the white noise assumption holds, the output has a shaped spectrum that pushes the quantizer noise gently toward high frequencies, without generating spurious tones [1].

When a DDSM is used in a mixed-signal system, such as a fractional-N synthesizer, its output spectrum can be distorted due to the nonlinearity of the subsequent stages [2], [18]–[21]. As shown in Fig. 1, distortion can appear in the output spectrum in the following ways:

1) harmonic tones when an ac input is applied;
2) elevated noise floor;
3) spurious tones.

Note that the spurious tones previously specified are typically due to the effect of the nonlinearity; the reader should differentiate between these tones and those that are inherent in the output of the DDSM itself [21]. Even if the modulator has an ideal smooth output spectrum, the distortion effects previously described can appear in the final output *after* the DDSM output signal passes through a subsequent nonlinearity [2], [19]–[21].

The spurs and the noise floor generated by the nonlinearity eventually degrade the performance of the synthesizer that uses the DDSM by decreasing the spurious-free dynamic range [22] and increasing the inband noise floor of the phase noise [2], respectively.

Swaminathan *et al.* [21] addressed the problem of spurious tones by proposing a digital requantizer that does not generate spurious tones after nonlinear distortion. It borrows ideas from dc-free codes [23], [24] and dynamic-element-matching tree-structured encoders [25], [26]. A set of quantization error signals is generated by design, so that the spectra of the total quantization error and its running sum do not contain spurious tones when applied to a memoryless truncated power series. The quantizer then implements first-order noise shaping without the use of a DDSM. This quantizer has been incorporated in a fractional-N frequency synthesizer [22] to demonstrate the concept. Although this technique minimizes the production of spurious tones, it does not address the problem of the elevated noise floor caused by the nonlinearity. Additional research is required to understand and correct the effects of nonlinearity.

In this paper, we consider the elevated noise floor. As in [21] and [22], the nonlinearity is assumed to be memoryless, and it can be represented by a polynomial with real coefficients corresponding to a truncated Taylor series. In this paper, the same truncated memoryless polynomial [21], [22] (of order three) is considered.

We describe only one step in understanding the effect of the prescribed memoryless nonlinearity on the DDSM spectrum, particularly predicting the elevated noise floor; further work is still needed to address the problem of spurious tones.

In order to approximate the power spectral density (PSD) of the output spectrum after distortion, a simple model of the DDSM is assumed, and results from previous work [27], [28]–[30] (particularly [27]) related to the theory of stochastic random processes are exploited. In the context of continuous-time Delta-Sigma Modulators (CT DSMs), Sankar and

Manuscript received April 21, 2009; revised August 05, 2009 and October 19, 2009; accepted November 25, 2009. Date of publication February 22, 2010; date of current version August 11, 2010. This work was supported in part by the Science Foundation Ireland under Grant 02/IN.1/I45 and Grant 08/IN1/I854, and in part by the University College Cork–University of California Scholarship Programme. This paper was recommended by Associate Editor G. Manganaro.

K. Hosseini was with the University College Cork, Cork, Ireland. He is now with the California Institute of Technology, Pasadena, CA 91125 USA (e-mail: hosseini@caltech.edu).

M. P. Kennedy is with the Department of Microelectronic Engineering, University College Cork and Tyndall National Institute, Cork, Ireland.

S. H. Lewis and B. Levy are with the Department of Electrical and Computer Engineering, University of California, Davis, CA 95616 USA.

Digital Object Identifier 10.1109/TCSI.2009.2039257

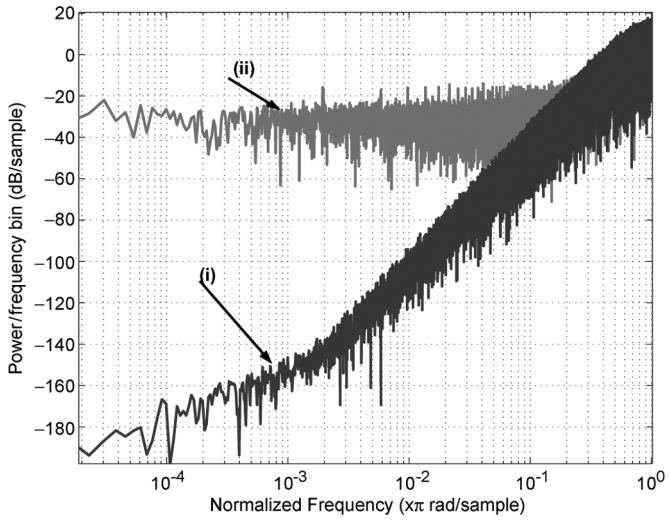

Fig. 2. PSD of a MASH 1-1-1 DDSM for the two cases of (i) without and (ii) with a nonlinear block. The nonlinearity is a polynomial of order five with arbitrarily chosen coefficients $a_0 = 0.001$, $a_1 = 1.001$, $a_2 = 0.01$, $a_3 = 0.001$, $a_4 = 0.0001$, and $a_5 = 0.00001$.

Pavan use the same method of analysis to predict the noise floor caused by the nonlinearity in the first integrator in a class of CT DSMs [31]. In Section II, a simplified model is described. In Section III, the analysis is explained. In Section IV, simulation results are presented to illustrate the analysis.

II. Background and Simplified Model

A. Simulation Example

In this section, we illustrate by simulation the generation of spurs and the elevated noise floor.

A third-order Multi stAge noise SHaping (MASH) DDSM of type 1-1-1 [32] with a constant input was simulated with and without a subsequent nonlinearity. In Fig. 2, the PSD [see plot (i)] of the DDSM output signal is plotted. A first-order-shaped least significant bit (LSB) dithering signal [4] has been added to the input in order to randomize the modulator output signal. The spectrum contains a dc term corresponding to the input and a shaped spectrum corresponding to the shaped quantization noise. Note that the spectrum of the quantization noise has been attenuated at low frequencies and amplified at high frequencies due to the noise-shaping property of the modulator.

In a fractional-N frequency synthesizer application, the spectrum can be distorted due to nonlinearities originating in the phase frequency detector and the charge pump [33]. In [21], the nonlinearity in the path of the quantization noise in a fractional-N synthesizer [34] has been modeled as a polynomial of order five, i.e.,

$$f(x) = a_0 + a_1 x + a_2 x^2 + a_3 x^3 + a_4 x^4 + a_5 x^5. \quad (1)$$

In order to illustrate the distortion resulting from such a nonlinearity, the output of the modulator taking integer values in the range $\{-3, -2, \ldots, 3, 4\}$ has been applied to a fifth-order polynomial with arbitrarily chosen coefficients: $a_0 = 0.001$, $a_1 = 1.001$, $a_2 = 0.01$, $a_3 = 0.001$, $a_4 = 0.0001$, and $a_5 = 0.00001$. The resulting spectrum is shown in plot (ii) in Fig. 2. The distortion manifests itself as an elevated noise floor (at ≈ -35 dB in this case) and some spurious tones above the noise floor that are not present in the original DDSM spectrum (i).

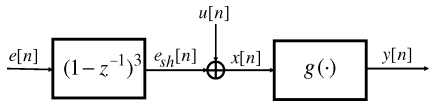

Fig. 3. Simplified model of a DDSM with $\mathrm{NTF}(z) = (1 - z^{-1})^3$ and $\mathrm{STF}(z) = 1$, cascaded with a memoryless output nonlinearity $g(\cdot)$. u represents the input to the DDSM, and e denotes the quantizer error.

B. Simplified Model

In the following, we will calculate the power spectral densities of DDSMs whose output signals are applied to memoryless polynomials of order three with constant coefficients. The goal is to find an expression for the PSD at the output of the nonlinear block, particularly to determine the noise floor.

In our model, we assume that the quantizer noise is both wide-sense stationary (WSS) and white. These two conditions are not automatically valid in DDSMs. However, recent theoretical work by Pamarti *et al.* shows that LSB dithering can be used in two classes of modulators, i.e., single-quantizer (SQ) and MASH DDSMs [4], [6], to ensure asymptotically that the quantization noise e has the following properties:

1) uniform distribution in the range $[-\Delta/2, \Delta/2]$, where $\Delta = 2/2^{\mathrm{QNOB}}$ is the step size of the quantizer and QNOB is the number of bits in the quantizer;
2) constant mean;
3) autocorrelation function $R_{ee}[n_0] = \sigma^2 \delta[n_0]$, where $\sigma^2 = \Delta^2/12$.

If the mean is constant and the autocorrelation function is a function of the delay between the two time stamps, then e can be assumed to be WSS [35]. In addition, the assumption that $R_{ee}[n_0] = \sigma^2 \delta[n_0]$ results in a white spectrum. Although the white noise assumption will allow us to predict the level of the noise floor, it will not permit the prediction of spurs.

In this paper, LSB dithering is applied, and we consider the DDSMs described in [4] and [6], so that we can asymptotically assume that the quantizer noise e is WSS. We will use Price's theorem [27], from the theory of stochastic random processes, to develop closed-form expressions for the noise floor.

With the aforementioned assumptions, a model can be built for the DDSM, as shown in Fig. 3. The noise source e modeling the quantizer noise and an input signal[1] u modeling the DDSM input are applied to the system.

The input e is applied to a filter $\mathrm{NTF}(z) = (1 - z^{-1})^3$ that represents the noise transfer function of the modulator. The output of the filter $e_{sh}[n]$ is added to the input signal u, assuming an all-pass signal transfer function $\mathrm{STF}(z) = 1$, and the resulting signal x is applied to the polynomial function $g(x) = a_0 + a_1 x + a_2 x^2 + a_3 x^3$, which models the nonlinearity that appears after the DDSM. We will calculate the PSD of the output y of the nonlinear block $g(\cdot)$.

[1]We consider a constant input.

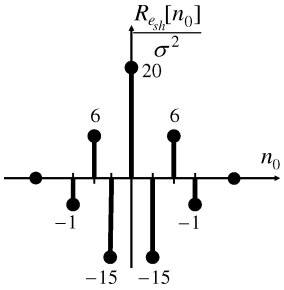

Fig. 4. Normalized autocorrelation function of the output of the filter.

The PSD of x with this simplified model is well known in the literature [1]. It has two components: 1) a component corresponding to the constant input u and 2) the shaped power spectrum of e, i.e., $\sigma^2|(1-z^{-1})^3|_{z=e^{j\omega}}|^2 = \sigma^2(2\sin(\omega/2))^6$, where $\sigma^2 = \Delta^2/12$ is the variance of e.

III. Analysis

To determine the PSD of the output y, the autocorrelation function at the input of the nonlinear block is required, because Price's theorem relates the autocorrelation functions at the input and output of a memoryless nonlinear function, whose input is a Gaussian process.

To simplify the computation and to make the result more useful in practice, we have assumed that the DDSM output is WSS. This ensures that the process at the output of the nonlinearity is also WSS. Note, however, that this is just an assumption; it is not a *requirement* of Price's theorem. The computation could also be performed for any nonstationary Gaussian input and would yield the nonstationary autocorrelation of the output.

For the filter shown in Fig. 3

$$e_{sh}[n] = e[n] - 3e[n-1] + 3e[n-2] - e[n-3]. \quad (2)$$

The mean of $e_{sh}[n]$ is zero. In order to determine the autocorrelation function $R_{e_{sh}}$ at the output of the filter, we compute

$$R_{e_{sh}}[n_0] = E\left[e_{sh}[n]e_{sh}[n-n_0]\right]. \quad (3)$$

After intermediate calculations, one obtains

$$\begin{aligned} R_{e_{sh}}[n_0] &= \sigma^2\left(20\delta[n_0] - 15\left(\delta[n_0-1] + \delta[n_0+1]\right)\right. \\ &\left. +6\left(\delta[n_0-2] + \delta[n_0+2]\right) - \left(\delta[n_0-3] + \delta[n_0+3]\right)\right) \quad (4) \end{aligned}$$

which is shown in Fig. 4. In deriving the preceding expression, we have assumed that $R_{ee}[n_0] = \sigma^2\delta[n_0]$. As can be seen from the figure, the autocorrelation of the shaped error contains seven nonzero impulses with the specified normalized amplitudes. For lags greater than three, the autocorrelation is zero. Assuming a constant input $u[n] = U$, one can write

$$m_x = U \quad (5)$$

$$R_x[n_0] = R_{e_{sh}}[n_0] + U^2. \quad (6)$$

Next, we calculate the autocorrelation function of the output of the nonlinear block.

A. Calculating the Autocorrelation Function of the Output of the Nonlinear Block Using Price's Theorem

The input–output relationship of the nonlinear block is defined by

$$y = g(x) = a_0 + a_1x + a_2x^2 + a_3x^3. \quad (7)$$

In order to find the output autocorrelation function $R_y[n_0]$, Price's theorem [27] is applied. Assuming that the input x is a Gaussian process, this theorem relates the input and output autocorrelation functions of the nonlinear block $g(\cdot)$ as follows:

$$\frac{\partial^k R_y[n_0]}{\partial R_x[n_0]^k} = E\left[\frac{\partial^k g(x_1)}{\partial x_1^k}\frac{\partial^k g(x_2)}{\partial x_2^k}\right] \quad (8)$$

where $x_1 = x[n]$ and $x_2 = x[n-n_0]$ are two instances of the input process x. The corresponding outputs are $y_1 = y[n]$ and $y_2 = y[n-n_0]$. $R_x[n_0]$ and $R_y[n_0]$ are defined by

$$R_x[n_0] = E\left[x[n]x[n-n_0]\right] \quad (9)$$

$$R_y[n_0] = E\left[y[n]y[n-n_0]\right]. \quad (10)$$

Starting with (8) and taking the first derivative, we write

$$\begin{aligned} \frac{\partial R_y[n_0]}{\partial R_x[n_0]} &= E\left[\frac{\partial g(x_1)}{\partial x_1}\frac{\partial g(x_2)}{\partial x_2}\right] \\ &= E\left[\left(a_1+2a_2x_1+3a_3x_1^2\right)\right. \\ &\quad \left.\times\left(a_1+2a_2x_2+3a_3x_2^2\right)\right]. \quad (11) \end{aligned}$$

Taking the second derivative gives

$$\begin{aligned} \frac{\partial R_y^2[n_0]}{\partial R_x[n_0]^2} &= E\left[(2a_2+6a_3x_1)(2a_2+6a_3x_2)\right] \\ &= 4a_2^2 + 12a_2a_3E[x_1] + 12a_2a_3E[x_2] \\ &\quad + 36a_3^2E[x_1x_2] \\ &= 4a_2^2 + 24a_2a_3U + 36a_3^2R_x[n_0] \quad (12) \end{aligned}$$

because $E(x) = U$. Integrating both sides gives

$$\begin{aligned} \frac{\partial R_y[n_0]}{\partial R_x[n_0]} &= 18a_3^2R_x^2[n_0] + \left(24a_2a_3U + 4a_2^2\right) \\ &\quad \times R_x[n_0] + C_1 \quad (13) \\ R_y[n_0] &= 6a_3^2R_x^3[n_0] + \left(12a_2a_3U + 2a_2^2\right)R_x^2[n_0] \\ &\quad + C_1R_x[n_0] + C_2. \quad (14) \end{aligned}$$

Equation (14) implies that R_y is a third-order polynomial in R_x.

Next, the values of the constants C_1 and C_2 are determined. From (13), one can write

$$C_1 = \frac{\partial R_y[n_0]}{\partial R_x[n_0]} - 18a_3^2R_x^2[n_0] - \left(24a_2a_3U + 4a_2^2\right)R_x[n_0]. \quad (15)$$

When $R_x[n_0] = E[x_1x_2] = E[x_1]E[x_2] = U^2$, then $R_y[n_0] = E[g(x_1)g(x_2)] = E[g(x_1)]E[g(x_2)]$, and $(\partial R_y[n_0]/\partial R_x[n_0]) = E[(\partial g(x_1)/\partial x_1)(\partial g(x_2)/\partial x_2)] = E[(\partial g(x_1)/\partial x_1)]E[(\partial g(x_2)/\partial x_2)]$.

We consider (15) in the case $R_x[n_0] = U^2$. The first term in (15) is calculated as follows:

$$\begin{aligned}\frac{\partial R_y[n_0]}{\partial R_x[n_0]} &= E\left[\left(a_1+2a_2x_1+3a_3x_1^2\right)\left(a_1+2a_2x_2+3a_3x_2^2\right)\right]\\ &= E\left[\left(a_1+2a_2x_1+3a_3x_1^2\right)\right]E\left[\left(a_1+2a_2x_2+3a_3x_2^2\right)\right]\\ &= \left(a_1+2a_2U+3a_3E\left[x_1^2\right]\right)^2\\ &= \left(a_1+2a_2U+3a_3\left(U^2+R_{e_{sh}}[0]+2UE[e_{sh}]\right)\right)^2\\ &= \left(a_1+2a_2U+3a_3(U^2+20\sigma^2)\right)^2. \end{aligned} \tag{16}$$

After substituting (16) into (15), the following expression is obtained for C_1:

$$\begin{aligned}C_1 = \left(a_1+2a_2U+3a_3(U^2+20\sigma^2)\right)^2\\ -\left(24a_2a_3U+4a_2^2\right)U^2-18a_3^2U^4.\end{aligned} \tag{17}$$

To find C_2, one can write

$$\begin{aligned}C_2 = R_y[n_0]-6a_3^2R_x^3[n_0]-\left(12a_2a_3U+2a_2^2\right)\\ \times R_x^2[n_0]-C_1R_x[n_0].\end{aligned} \tag{18}$$

The preceding equation is examined when $R_x[n_0] = U^2$. $R_y[n_0]$ is calculated as follows:

$$\begin{aligned}&R_y[n_0]|_{R_x[n_0]=U^2}\\ &= E\left[\left(a_0+a_1x_1+a_2x_1^2+a_3x_1^3\right)\right.\\ &\qquad\left.\times\left(a_0+a_1x_2+a_2x_2^2+a_3x_2^3\right)\right]\\ &= E\left[\left(a_0+a_1x_1+a_2x_1^2+a_3x_1^3\right)\right]\\ &\quad\times E\left[\left(a_0+a_1x_2+a_2x_2^2+a_3x_2^3\right)\right]\\ &= \left(a_0+a_1U+a_2(U^2+20\sigma^2)+a_3E[x^3]\right)^2\\ &= \left(a_0+a_1U+a_2(U^2+20\sigma^2)+a_3(U^3+60U\sigma^2)\right)^2.\end{aligned} \tag{19}$$

After substituting (19) into (18), the following expression is obtained for C_2:

$$\begin{aligned}C_2 = R_y[n_0]|_{R_x[n_0]=U^2}-6a_3^2U^6\\ -\left(12a_2a_3U+2a_2^2\right)U^4-C_1U^2.\end{aligned} \tag{20}$$

In (16) and (20), we have used the fact that $E[e_{sh}] = E[e_{sh}^3] = 0$, because e_{sh} is assumed to be a zero-mean Gaussian process [35].

B. Final Computations

Substituting $R_x[n_0] = U^2 + R_{e_{sh}}[n_0]$ into (14), we obtain, after intermediate calculations

$$\begin{aligned}R_y[n_0] = A_x\delta[n_0]+B_x\left[\delta[n_0-1]+\delta[n_0+1]\right]\\ +C_x\left[\delta[n_0-2]+\delta[n_0+2]\right]\\ +D_x\left[\delta[n_0-3]+\delta[n_0+3]\right]+E_x\end{aligned} \tag{21}$$

where

$$\begin{aligned}A_x &= 6a_3^2\sigma^6 20^3+\left(18a_3^2U^2+2a_2^2+12a_2a_3U\right)\sigma^4 20^2\\ &\quad+\left(18a_3^2U^4+\left(4a_2^2+24a_2a_3U\right)U^2+C_1\right)\sigma^2 20\\ B_x &= -6a_3^2\sigma^6 15^3+\left(18a_3^2U^2+2a_2^2+12a_2a_3U\right)\sigma^4 15^2\\ &\quad-\left(18a_3^2U^4+\left(4a_2^2+24a_2a_3U\right)U^2+C_1\right)\sigma^2 15\\ C_x &= 6a_3^2\sigma^6 6^3+\left(18a_3^2U^2+2a_2^2+12a_2a_3U\right)\sigma^4 6^2\\ &\quad+\left(18a_3^2U^4+\left(4a_2^2+24a_2a_3U\right)U^2+C_1\right)\sigma^2 6\\ D_x &= -6a_3^2\sigma^6+\left(18a_3^2U^2+2a_2^2+12a_2a_3U\right)\sigma^4\\ &\quad-\left(18a_3^2U^4+\left(4a_2^2+24a_2a_3U\right)U^2+C_1\right)\sigma^2\\ E_x &= C_2+C_1U^2+U^4\left(2a_2^2+12a_2a_3U\right)+6a_3^2U^6.\end{aligned} \tag{22}$$

Taking the discrete-time Fourier transform of (21) gives its PSD

$$\begin{aligned}S_{yy}(e^{j\omega}) = A_x+2B_x\cos(\omega)+2C_x\cos(2\omega)\\ +2D_x\cos(3\omega)+2\pi E_x\delta(\omega).\end{aligned} \tag{23}$$

Consider the case when there is no nonlinearity after the DDSM. In this case, $a_0 = a_2 = a_3 = 0$, and $a_1 = 1$. Examining this condition in (23) gives the PSD in the conventional linear case, i.e., $S(e^{j\omega}) = 2\pi U^2 + \sigma^2(2\sin(\omega/2))^6$.

Next, consider (23) around $\omega \approx 0$, excluding the dc component. At low frequencies, close to dc, $\cos(\omega) \approx 1$, and (23), excluding the dc term, becomes

$$S_{yy1}(e^{j\omega}) \approx A_x+2B_x+2C_x+2D_x \tag{24}$$

which is no longer zero[2] when a_0, a_2, $a_3 \neq 0$. This raises the low-frequency part of the spectrum. As long as ω is small, (24) shows up in the spectrum as a constant offset, as will be confirmed by simulation in the next section.

IV. MATLAB SIMULATIONS

In this section, the simplified model is shown in Fig. 3, and then real SQ and MASH DDSMs are simulated in MATLAB. The simulation results and predictions from the analysis are overlaid.

A. Simulation of the Simplified Model and an SQ-DDSM

1) Simplified Model: A white noise signal with a uniform distribution in the range $[-\Delta/2, \Delta/2]$ is generated using the *rand* function and applied as the input e. Here, $\Delta = 2/2^{\mathrm{QNOB}}$, where QNOB represents the number of bits of the quantizer.

The "periodogram" method [36], with a Hanning window w of length $L = \mathrm{NFFT}$, was used to generate the PSD using

$$Y[k] = \frac{\left|\sum_{n=0}^{L-1} y[n]w[n]e^{-j\frac{2\pi}{L}nk}\right|^2}{\sum_{n=0}^{L-1}|w[n]|^2}. \tag{25}$$

Plot (i) in Fig. 5 shows the output PSD with no nonlinearity (a_0, a_2, $a_3 = 0$ and $a_1 = 1$). In this example, QNOB $= 4$, $\Delta = 1/8$, $M = 2^{24}$, $U = 1/128$, and $L = \mathrm{NFFT} = 2^{18}$.

As expected for a third-order modulator with no nonlinearity, the noise power is spread toward high frequencies with a slope of 60 dB/dec. The solid curve shows the theoretical prediction

[2]This expression is zero in the linear case, meaning that the quantizer noise is rejected around $\omega = 0$.

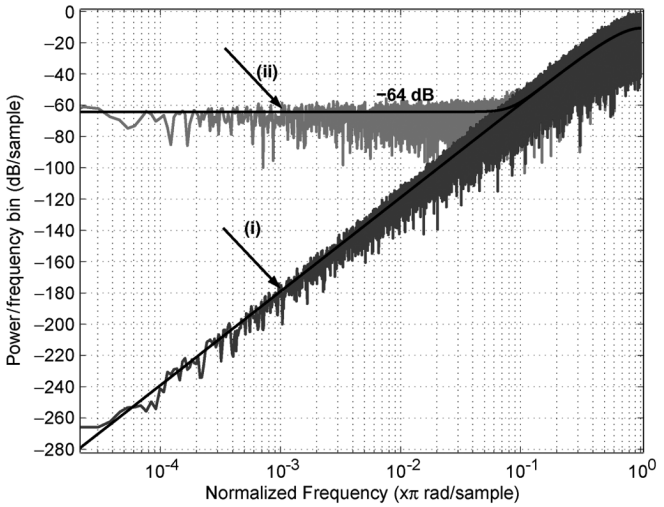

Fig. 5. PSD of the output of the block diagram shown in Fig. 3 for two cases of (i) without and (ii) with a third-order nonlinearity, where $a_0 = 0.005$, $a_1 = 1.01$, $a_2 = 0.011$ $a_3 = 0.0011$. $U = 1/128$, $\mathrm{QNOB} = 4$, and $M = 2^{24}$. The solid curves show the theoretical predictions.

given by $\sigma^2(2\sin(\omega/2)^6)$, and the gray plot shows the simulation result.

Plot (ii) in Fig. 5 shows the result when the nonlinearity has the following arbitrarily chosen coefficients: $a_0 = 0.005$, $a_1 = 1.01$, $a_2 = 0.011$, and $a_3 = 0.0011$. The noise floor appears at -64 dB due to the nonlinearity; the simulation matches the prediction.

2) SQ-DDSM: The block diagram of an SQ-DDSM [6] with a midtread quantizer is shown in Fig. 6(a). The modulator implements the following signal and noise transfer functions:

$$\mathrm{STF}(z) = z^{-3}$$
$$\mathrm{NTF}(z) = (1 - z^{-1})^3.$$

In the quantizer, each quantization step is of length $\Delta_1 = 2M/2^{\mathrm{QNOB}}$, and the output y_Q takes discrete values from $N_{\min}\Delta_1$ to $N_{\max}\Delta_1$. An example transfer characteristic is shown with $N_{\min} = -2$ and $N_{\max} = 2$.

In the simulation, $N_{\min}\Delta_1 = -M + (M/2^{\mathrm{QNOB}-1})$, and $N_{\max}\Delta_1 = M$. The output of the quantizer has been divided by M in order to match the output ranges of the SQ-DDSM and the model shown in Fig. 3.

The simulations were repeated with the same parameters used for generating Fig. 5 for the SQ-DDSM modulator shown in Fig. 6. An LSB dithering signal is added to the input of the modulator to whiten the quantizer noise [6]. Simulation results are shown in Fig. 7 for two cases, i.e., (i) without and (ii) with the polynomial nonlinearity.

Plot (i) is for the case with no nonlinearity. With dithering, the spectrum is free of spurious tones. Plot (ii) illustrates simulation results for the case where a nonlinearity is present. As expected, the noise floor rises, and the mathematical prediction of -64 dB using the simplified model matches the simulation for the real SQ-DDSM modulator.

Note that Price's theorem assumes a Gaussian input. In Fig. 8(a) and (b), the probability distribution function (pdf) of the input x of the nonlinear block is plotted for the simplified

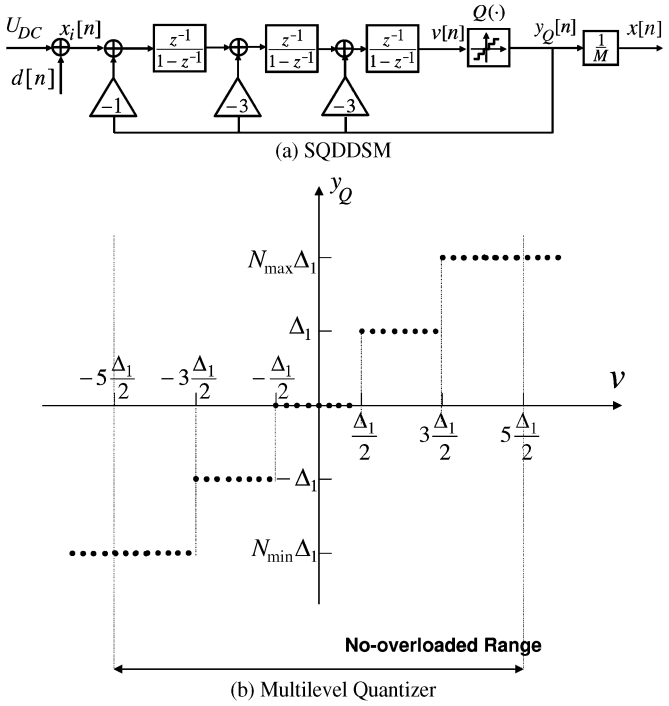

Fig. 6. (a) Block diagram of a third-order SQ-DDSM. (b) Example transfer characteristic of a midtread multilevel quantizer with $N_{\min} = -2$ and $N_{\max} = 2$.

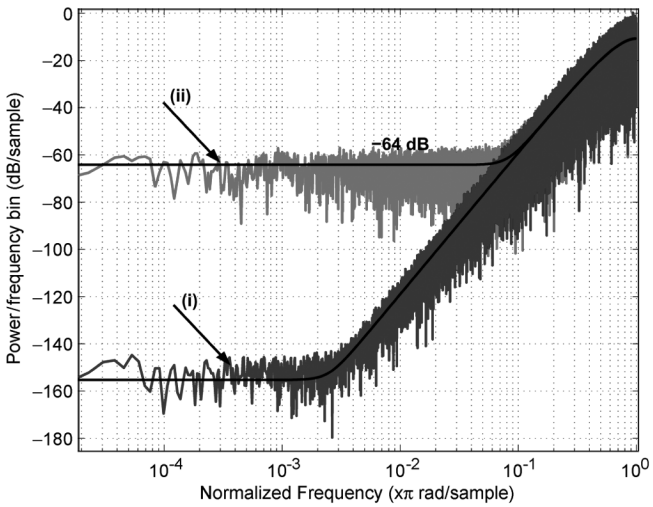

Fig. 7. PSD of the output of the nonlinearity located after the third-order SQ-DDSM shown in Fig. 6(a) for the two cases of (i) no nonlinearity and (ii) $a_0 = 0.005$, $a_1 = 1.01$, $a_2 = 0.011$, and $a_3 = 0.0011$. In both cases, $U_{\mathrm{DC}} = M/128$, $\mathrm{QNOB} = 4$, and $M = 2^{24}$. The dither contribution is also considered.

and real SQ-DDSM with $U = 1/128$. The error e has a uniform distribution by design. After filtering (summations of the delayed versions of e), the resulting distribution tends toward Gaussian, due to the central limit theorem [35].

Note that, when the central limit theorem is invoked to approximate a sum of independent identically distributed (i.i.d.) random variables by a Gaussian random variable, only a small number of random variables is needed to obtain a good approximation of the central part of the Gaussian distribution; it is only the approximation of the tails that requires a large number of

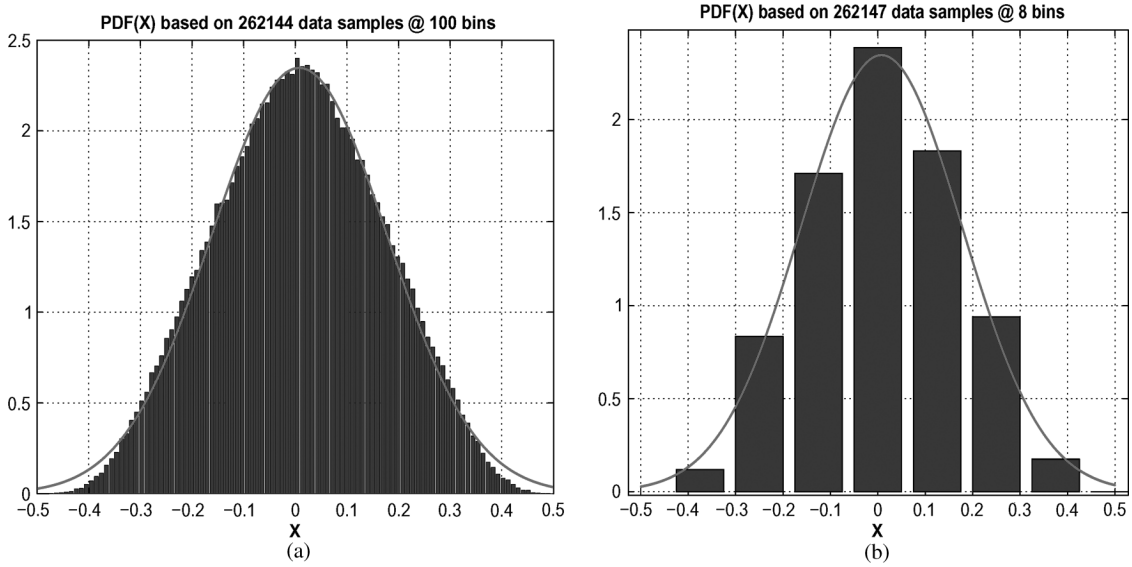

Fig. 8. PDF of the input x to the nonlinear block for two cases: (a) simplified model and (b) SQ-DDSM. The solid curves are plotted using the formula of the Gaussian distribution with the empirical mean of $U = 1/2^7$ and a standard deviation of 0.17. The standard deviation is estimated to be $\sigma_{ee}\sqrt{1+3^2+3^2+1} = ((1/8)/\sqrt{12})\sqrt{20} = 0.161$.

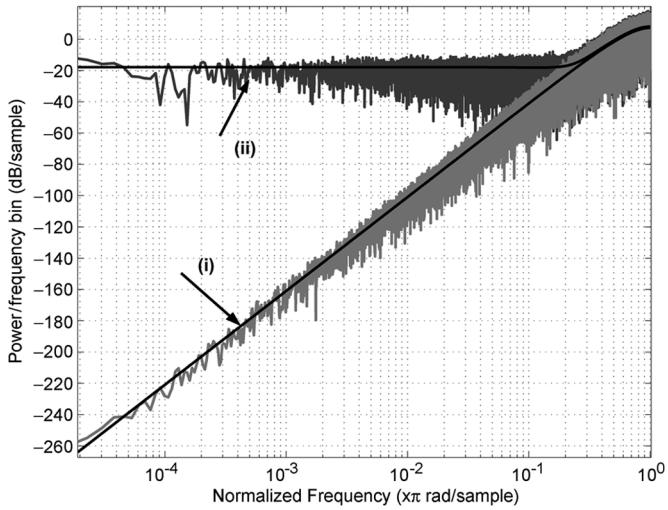

Fig. 9. PSD of the output of the block diagram shown in Fig. 3 for the two cases of (i) without nonlinearity and (ii) with third-order nonlinearity, where $a_0 = 0.001$, $a_1 = 1.05$, $a_2 = 0.031$, and $a_3 = 0.003$. $U = 1/2$, $\mathrm{QNOB} = 1$, and $M = 2^{16}$. The solid curves show the theoretical predictions.

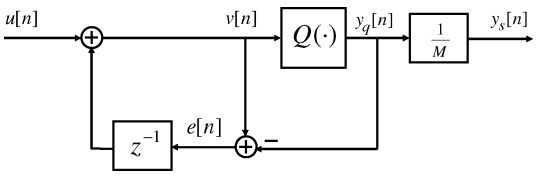

Fig. 10. Block diagram of the EFM used in Fig. 11.

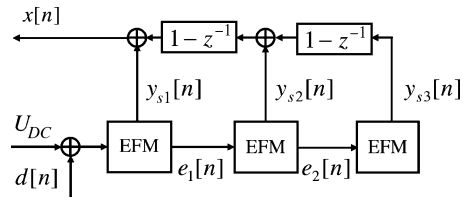

Fig. 11. Block diagram of the simulated MASH 1-1-1 DDSM.

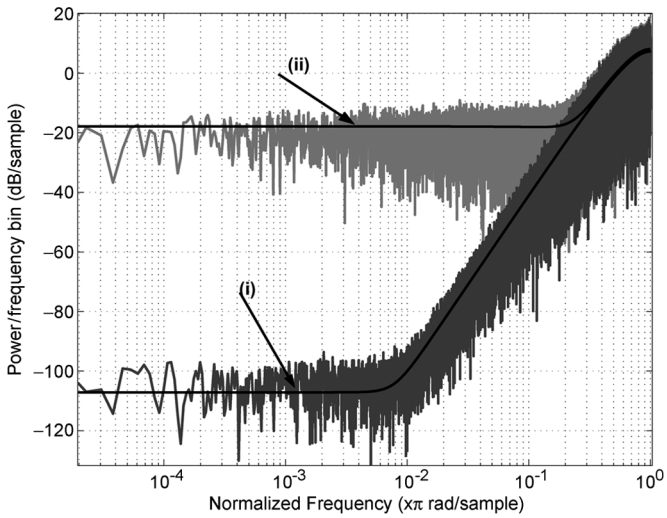

Fig. 12. PSD of the output of the simulated MASH 1-1-1 DDSM for the two cases of (i) without nonlinearity and (ii) with third-order nonlinearity, where $a_0 = 0.001$, $a_1 = 1.05$, $a_2 = 0.031$, and $a_3 = 0.003$. $U_{\mathrm{DC}} = M/2$, $\mathrm{QNOB} = 1$, and $M = 2^{16}$. The solid curves show the theoretical predictions.

random variables. However, since Price's theorem concerns the evaluation of expectations where the contribution of the tails of probability distributions is small, it is reasonable to employ a Gaussian approximation for $e_{sh}[n]$, even though it is a sum of only *four* i.i.d. random variables in this example.

B. Simulation of the Simplified Model and a MASH DDSM

1) Simplified Model: In this section, we consider the simplified model and a third-order MASH 1-1-1 DDSM. The model is simulated with the following parameters: $U = 1/2$, $M = 2^{16}$,

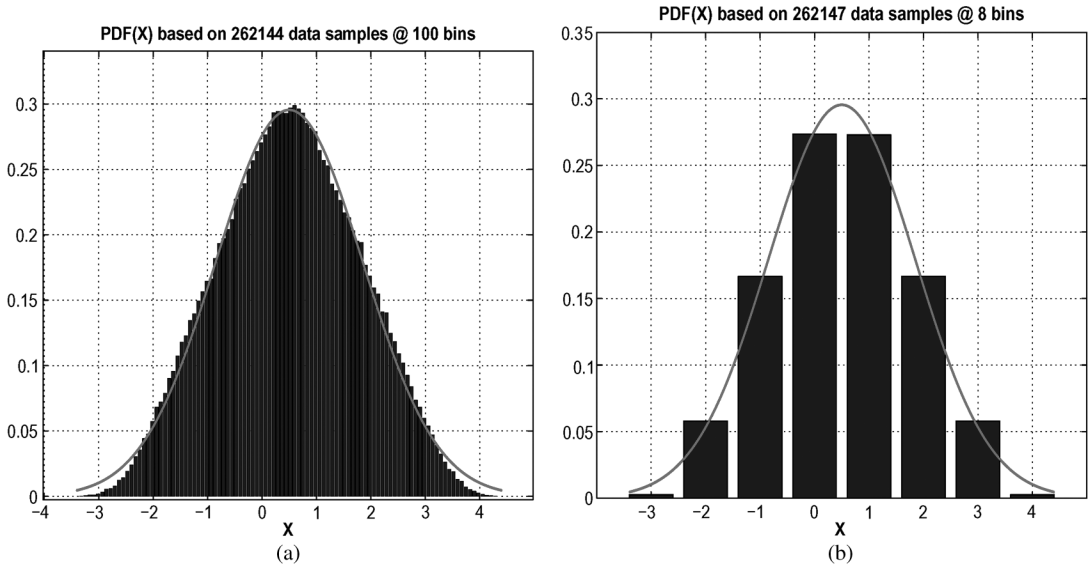

Fig. 13. PDF of the input x to the nonlinear block for two cases: (a) simplified model and (b) MASH DDSM. The solid curves are plotted using the formula of the Gaussian distribution with a mean of one-half and a standard deviation of 1.35.

and $\mathrm{QNOB} = 1$. A white noise signal with a uniform distribution in the range [0 1] was generated using the *rand* function and is applied as the input e.

Plot (i) in Fig. 9 shows the output PSD with no nonlinearity. As expected for a third-order modulator with no nonlinearity, the noise power is spread toward high frequencies with a slope of 60 dB/dec.

Next, a simulation result is presented when the nonlinearity has the following arbitrarily chosen coefficients: $a_0 = 0.001$, $a_1 = 1.05$, $a_2 = 0.031$, and $a_3 = 0.003$. The simulation result is shown in plot (ii) in Fig. 9. The noise floor appears at -18 dB due to the nonlinearity; the simulation matches the prediction.

Next, we present simulation results for a real MASH 1-1-1.

2) MASH: The block diagram of the simulated third-order MASH DDSM is shown in Fig. 10. It consists of three first-order error feedback modulators (EFMs) of the type shown in Fig. 11. The 1-bit quantizer in the EFM implements the following operation:

$$Q(v) = \begin{cases} 0, & v < M \\ M, & v \geq M \end{cases}, \tag{26}$$

where M is the step size of the quantizer.

The modulator is simulated with the following parameters: $M = 2^{16}$, $\mathrm{QNOB} = 1$, and $U_{\mathrm{DC}} = M/2$. An LSB dithering signal is added to the input of the modulator to whiten the quantizer noise [4]. The resulting spectra for two cases of (i) without and (ii) with a subsequent nonlinearity are shown in Fig. 12.

Plot (i) is for the case with no nonlinearity. With dithering, the spectrum is free of spurious tones. Plot (ii) illustrates simulation results for the case where a nonlinearity is present. As expected, the noise floor rises to -18 dB, and the mathematical prediction using the simplified model matches the simulation for the real MASH modulator.

In Fig. 13, the pdf of the input signal x applied to the nonlinearity is plotted for the simplified model and the real MASH DDSM. In both cases, a Gaussian can be fitted with distributions plotted from the simulation.

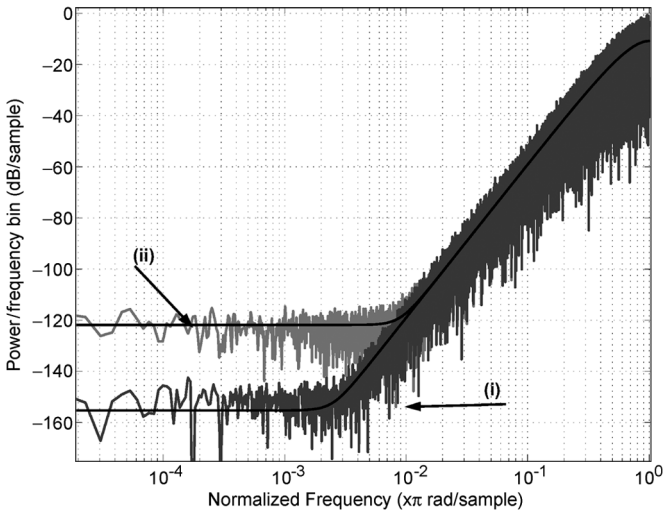

Fig. 14. PSD of the output of the nonlinearity located after the third-order SQ-DDSM shown in Fig. 6(a) for two cases: (i) no nonlinearity and (ii) $a_0 = 0.00003011$, $a_1 = 1.0000521$, $a_2 = -0.0000133$, and $a_3 = -0.00003373$. In both cases, $U_{\mathrm{DC}} = M/128$, $\mathrm{QNOB} = 4$, and $M = 2^{24}$. The dither contribution is also considered.

The simulations were repeated with the coefficients given in [21]; the analysis correctly predicts the noise floor. Note that averaging could be used to reduce the variance of the simulated result and, thereby, bring it closer to the prediction.

The simulations were repeated for both types of modulators for smaller levels of nonlinearity. In the case of the SQ-DDSM, the following parameters were used: $a_0 = 0.00003011$, $a_1 = 1.0000521$, $a_2 = -0.0000133$, $a_3 = -0.00003373$, $U_{\mathrm{DC}} = M/128$, $\mathrm{QNOB} = 4$, and $M = 2^{24}$. In addition, for the MASH DDSM, the following parameters were used: $a_0 = 0.000322$, $a_1 = 1.00321$, $a_2 = -0.00003$, $a_3 = -0.000033$, $U_{\mathrm{DC}} =$

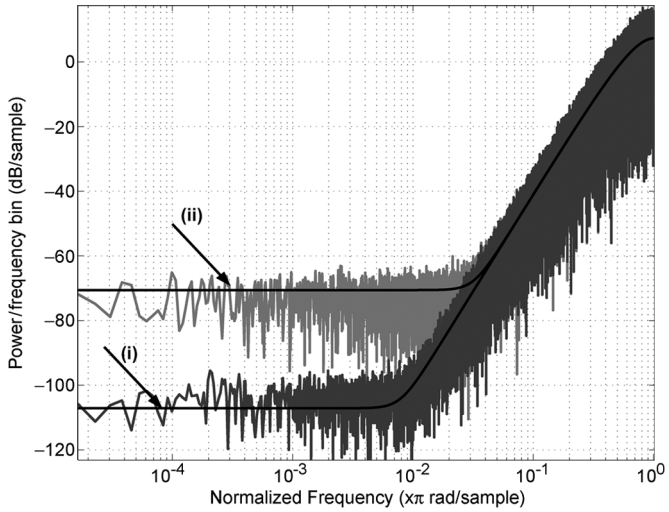

Fig. 15. PSD of the output of the simulated MASH 1-1-1 DDSM for the two cases of (i) without nonlinearity and (ii) with third-order nonlinearity, where $a_0 = 0.000322$, $a_1 = 1.00321$, $a_2 = -0.00003$, and $a_3 = -0.000033$. $U_{\rm DC} = M/2$, $\rm QNOB = 1$, and $M = 2^{16}$. The solid curves show the theoretical predictions.

$M/128$, $\rm QNOB = 1$, and $M = 2^{16}$. The results are shown in Figs. 14 and 15. The simulation and analysis results match, as expected.

V. Conclusion

In this paper, we have used Price's theorem to analyze the effects of a memoryless polynomial nonlinearity on the PSD of a DDSM. As observed in the literature, distortion after the DDSM causes the generation of harmonic and spurious tones, as well as raising the noise floor. The principal contribution of this paper is to predict the level of the noise floor when a constant input is applied. The analysis has assumed a noise transfer function of order three and a memoryless third-order polynomial nonlinearity. The analysis has accurately predicted the noise floor when the input to the nonlinearity has a Gaussian distribution. A similar approach can be used for higher order polynomials although the algebra becomes more involved.

Acknowledgment

The authors would like to thank the reviewers and the Associate Editor for their constructive feedback.

References

[1] S. R. Norsworthy, R. Schreier, and G. C. Temes, *Delta–Sigma Data Converters: Theory, Design, and Simulation*. New York: IEEE Press, 1997.

[2] B. De Muer and M. Steyaert, "A CMOS monolithic $\Delta\Sigma$-controlled fractional-N frequency synthesizer for DCS-1800," *IEEE J. Solid-State Circuits*, vol. 37, no. 7, pp. 835–844, Jul. 2002.

[3] D. Reefman, J. Reiss, E. Janssen, and M. Sandler, "Description of limit cycles in sigma–delta modulators," *IEEE Trans. Circuits Syst. I, Reg. Papers*, vol. 52, no. 6, pp. 1211–1223, Jun. 2005.

[4] S. Pamarti and I. Galton, "LSB dithering in MASH delta–sigma D/A converters," *IEEE Trans. Circuits Syst. I, Reg. Papers*, vol. 54, no. 4, pp. 779–790, Apr. 2007.

[5] I. Galton, "One-bit dithering in delta–sigma modulator-based D/A conversion," in *Proc. IEEE ISCAS*, 1993, vol. 2, pp. 1310–1313.

[6] S. Pamarti, J. Welz, and I. Galton, "Statistics of the quantization noise in 1-bit dithered single-quantizer digital delta–sigma modulators," *IEEE Trans. Circuits Syst. I, Reg. Papers*, vol. 54, no. 3, pp. 492–503, Mar. 2007.

[7] M. Annovazzi, V. Colonna, G. Gandolfi, F. Stefani, and A. Baschirotto, "A low-power 98-dB multibit audio DAC in a standard 3.3-V 0.35-μm CMOS technology," *IEEE J. Solid-State Circuits*, vol. 37, no. 7, pp. 825–834, Jul. 2002.

[8] S. R. Norsworthy, "Effective dithering of sigma–delta modulators," in *Proc. ISCAS*, May 1992, vol. 3, pp. 1304–1307.

[9] P. Wong and R. Gray, "Sigma–delta modulation with i.i.d. Gaussian inputs," *IEEE Trans. Inf. Theory*, vol. 36, no. 4, pp. 784–798, Jul. 1990.

[10] W. Chou, "Sigma delta and multi-stage sigma delta modulation with inside loop dithering," in *Proc. Int. Conf. Acoust., Speech, Signal Process.*, Apr. 1991, vol. 3, pp. 1953–1956.

[11] W. Chou and R. M. Gray, "Dithering and its effects on sigma–delta and multistage sigma–delta modulation," *IEEE Trans. Inf. Theory*, vol. 37, no. 3, pp. 500–513, May 1991.

[12] M. Motamed, S. Sanders, and A. Zakhor, "The double loop sigma delta modulator with unstable filter dynamics: Stability analysis and tone behavior," *IEEE Trans. Circuits Syst. II, Analog Digit. Signal Process.*, vol. 43, no. 8, pp. 549–559, Aug. 1996.

[13] M. Kozak and I. Kale, *Oversampled Delta–Sigma Modulators, Analysis, Applications and Novel Topologies*. Boston, MA: Kluwer, 2003.

[14] M. J. Borkowski, T. A. D. Riley, J. Hakkinen, and J. Kostamovaara, "A practical delta sigma modulator design method based on periodical behavior analysis," *IEEE Trans. Circuits Syst. II, Exp. Briefs*, vol. 52, no. 10, pp. 626–630, Oct. 2005.

[15] K. Hosseini and M. P. Kennedy, "Mathematical analysis of a prime modulus quantizer MASH digital delta–sigma modulator," *IEEE Trans. Circuits Syst. II, Exp. Briefs*, vol. 54, no. 12, pp. 1105–1109, Dec. 2007.

[16] K. Hosseini and M. P. Kennedy, "Maximum sequence length MASH digital delta sigma modulators," *IEEE Trans. Circuits Syst. I, Reg. Papers*, vol. 54, no. 12, pp. 2628–2638, Dec. 2007.

[17] K. Hosseini and M. P. Kennedy, "Architectures for maximum sequence length digital delta–sigma modulators," *IEEE Trans. Circuits Syst. II, Exp. Briefs*, vol. 55, no. 10, pp. 1104–1108, Nov. 2008.

[18] B. De Muer and M. Steyaert, "On the analysis of $\Delta\Sigma$ fractional-N frequency synthesizers for high-spectral purity," *IEEE Trans. Circuits Syst. II, Analog Digit. Signal Process.*, vol. 50, no. 11, pp. 784–793, Nov. 2003.

[19] H. Hedayati, B. Bakkaloglu, and W. Khalil, "Closed-loop nonlinear modeling of wideband $\Sigma\Delta$ fractional-N frequency synthesizers," *IEEE Trans. Microw. Theory Tech.*, vol. 54, no. 10, pp. 3654–3663, Oct. 2006.

[20] W. Khalil, H. Hedayati, B. Bakkaloglu, and S. Kiaei, "(Invited) analysis and modeling of noise folding and spurious emission in wideband fractional-n synthesizers," in *Proc. IEEE RFIC*, Apr. 2008, pp. 291–294.

[21] A. Swaminathan, A. Panigada, E. Masry, and I. Galton, "A digital requantizer with shaped requantization noise that remains well behaved after nonlinear distortion," *IEEE Trans. Signal Process.*, vol. 55, no. 11, pp. 5382–5394, Nov. 2007.

[22] K. Wang, A. Swaminathan, and I. Galton, "Spurious-tone suppression techniques applied to a wide-bandwidth 2.4 GHz fractional-N PLL," in *Proc. IEEE Int. Solid-State Circuits Conf. Dig. Tech. Papers*, Feb. 2008, pp. 342–618.

[23] B. Marcus and P. Siegel, "On codes with spectral nulls at rational submultiples of the symbol frequency," *IEEE Trans. Inf. Theory*, vol. IT-33, no. 4, pp. 557–568, Jul. 1987.

[24] G. Pierobon, "Codes for zero spectral density at zero frequency," *IEEE Trans. Inf. Theory*, vol. IT-30, no. 2, pp. 435–439, Mar. 1984.

[25] I. Galton, "Spectral shaping of circuit errors in digital-to-analog converters," *IEEE Trans. Circuits Syst. II, Analog Digit. Signal Process.*, vol. 44, no. 10, pp. 808–817, Oct. 1997.

[26] E. Fogleman and I. Galton, "A digital common-mode rejection technique for differential analog-to-digital conversion," *IEEE Trans. Circuits Syst. II, Analog Digit. Signal Process.*, vol. 48, no. 3, pp. 255–271, Mar. 2001.

[27] R. Price, "A useful theorem for nonlinear devices having Gaussian inputs," *IEEE Trans. Inf. Theory*, vol. IT-4, no. 2, pp. 69–72, Jun. 1958.

[28] J. Barrett and D. Lampard, "An expansion for some second-order probability distributions and its application to noise problems," *IEEE Trans. Inf. Theory*, vol. IT-1, no. 1, pp. 10–15, Mar. 1955.

[29] J. J. Bussgang, Crosscorrelation functions of amplitude-distorted Gaussian signals Res. Lab. Electron., MIT, Cambridge, MA, Tech. Rep. 216, 1952.

[30] R. Pawula, "A modified version of Price's theorem," *IEEE Trans. Inf. Theory*, vol. IT-13, no. 2, pp. 285–288, Apr. 1967.
[31] P. Sankar and S. Pavan, "Analysis of integrator nonlinearity in a class of continuous-time delta-sigma modulators," *IEEE Trans. Circuits Syst. II, Express Briefs*, vol. 54, no. 12, pp. 1125–1129, Dec. 2007.
[32] T. A. D. Riley, M. A. Copland, and T. A. Kwasniewski, "Delta–Sigma modulation in fractional-N frequency synthesis," *IEEE J. Solid-State Circuits*, vol. 28, no. 5, pp. 553–559, May 1993.
[33] B. D. Muer and M. Steyaert, *CMOS Fractional-N Synthesizers: Design for High Spectral Purity and Monolithic Integration*. Norwell, MA: Kluwer, 2003.
[34] A. Swaminathan, K. Wang, and I. Galton, "A wide-bandwidth 2.4 GHz ISM band fractional-N PLL with adaptive phase noise cancellation," *IEEE J. Solid-State Circuits*, vol. 42, no. 12, pp. 2639–2650, Dec. 2007.
[35] A. Papoulis and S. U. Pillai, *Probability, Random Variables and Stochastic Processes*, 4th ed. New York: McGraw-Hill, 2001.
[36] A. V. Oppenheim, R. W. Schafer, and J. R. Buck, *Discrete-Time Signal Processing*. Englewood Cliffs, NJ: Prentice-Hall, 1999.

Kaveh Hosseini (S'07–M'10) received the B.Sc. degree in electronic engineering from the University of Tabriz, Tabriz, Iran, in 2002, the M.Sc. degree from Sharif University of Technology, Tehran, Iran, in 2004, and the Ph.D. degree from the University College Cork, Cork, Ireland, in 2009.

He spent the academic year 2007–2008 in the University of California, Davis, under an exchange scholarship supported by the University College Cork and the University of California. He is currently a Postdoctoral Scholar with the Department of Electrical Engineering, California Institute of Technology, Pasadena. His research interests include circuit design and signal processing.

Dr. Hosseini was the recipient of the Outstanding Doctoral Research Publication Award by Microelectronic Industry Design Association (MIDAS, Ireland) for the paper entitled "Maximum Sequence Length MASH Digital Delta–Sigma Modulators" in IEEE TRANSACTIONS ON CIRCUITS AND SYSTEMS—I: REGULAR PAPERS in 2007.

Michael Peter Kennedy (S'84–M'91–SM'95–F'98) received the B.E. degree in electronics from the National University of Ireland, Dublin, Ireland, in 1984 and the M.S. and Ph.D. degrees from the University of California (UC Berkeley), Berkeley, in 1987 and 1991, respectively.

He was a Design Engineer with Philips Electronics; a Post-Doctoral Research Engineer with the Electronics Research Laboratory, UC Berkeley; and a Professeur Invité with Federal Institute of Technology Lausanne (EPFL), Lausanne, Switzerland. From 1992 to 2000, he was with the faculty of the Department of Electronic and Electrical Engineering, University College Dublin, Dublin, where he taught electronic circuits and computer-aided circuit analysis, and directed the undergraduate Electronics Laboratory. In 2000, he joined the University College Cork (UCC), Cork, Ireland, as a Professor and Head of the Department of Microelectronic Engineering. He was elected Dean of the Faculty of Engineering, UCC, in 2003 and appointed Vice-President for Research Policy and Support in 2005. He has authored more than 250 papers in the area of nonlinear circuits and taught courses on nonlinear dynamics and chaos in U.K., Switzerland, Italy, and Hungary. He is the holder of four patents. His research interests are the simulation, design, and analysis of nonlinear dynamical systems for applications in communications and signal processing.

Dr. Kennedy has been a member of the Royal Irish Academy since 2004. He served as an Associate Editor for the IEEE TRANSACTIONS ON CIRCUITS AND SYSTEMS from 1993 to 1995 and from 1999 to 2004. He was the recipient of the 1991 Best Paper Award from the *International Journal of Circuit Theory and Applications*, the Best Paper Award at the European Conference on Circuit Theory and Design 1999, the IEEE Third Millenium Medal, the IEEE Circuits and Systems Society Golden Jubilee Medal in 2000, and the inaugural Parsons Medal for Engineering Sciences of the Royal Irish Academy in 2001.

Stephen H. Lewis (S'85–M'88–SM'97–F'01) received the B.S. degree in electrical engineering from Rutgers University, New Brunswick, NJ, in 1979, the M.S. degree in electrical engineering from Stanford University, Stanford, CA, in 1980, and the Ph.D. degree in electrical engineering from the University of California, Berkeley, in 1987.

From 1980 to 1982, he was with Bell Laboratories, Whippany, NJ, where he was involved in circuit design for magnetic recording. In 1988, he rejoined Bell Laboratories, Reading, PA, where he concentrated on the design of analog-to-digital converters. In 1991, he joined the Department of Electrical and Computer Engineering, University of California, Davis, where he is currently a Professor. He is also a coauthor of a college textbook on analog integrated circuits. His research interests include data conversion, signal processing, and analog circuit design.

Bernard C. Levy (S'78–M'78–SM'90–F'94) received the Diploma of Ingénieur Civil des Mines from the Ecole Nationale Supérieure des Mines, Paris, France, in 1974 and the Ph.D. degree in electrical engineering from Stanford University, Stanford, CA, in 1979.

From July 1979 to June 1987, he was an Assistant and then an Associate Professor with the Department of Electrical Engineering and Computer Science, Massachusetts Institute of Technology, Cambridge. Since July 1987, he has been with the University of California, Davis (UC Davis), where he is currently a Professor of electrical engineering with the Department of Electrical and Computer Engineering and a member of the Graduate Group in Applied Mathematics. From 1996 to 2000, he was the Chair of the Department of Electrical and Computer Engineering, UC Davis. He was a Visiting Scientist with the Institut de Recherche en Informatique et Systémes Aléatoires (IRISA), Rennes, France, from January to July 1993, and the Institut National de Recherche en Informatique et Automatique (INRIA), Rocquencourt, France, from September to December 2001. He is the author of the book *Principles of Signal Detection and Parameter Estimation* (New York, NY: Springer, 2008). He has been an Associate Editor for the *EURASIP Journal on Advances in Signal Processing*. His research interests include statistical signal processing, estimation, detection, and multidimensional signal processing.

Dr. Levy is a member of the Society for Industrial and Applied Mathematics and the Acoustical Society of America. He served as an Associate Editor for the IEEE TRANSACTIONS ON CIRCUITS AND SYSTEMS—I: REGULAR PAPERS and the IEEE TRANSACTIONS ON CIRCUITS AND SYSTEMS—II: EXPRESS BRIEFS. He was a member of the Image and Multidimensional Signal Processing technical committee of the IEEE Signal Processing Society from 1992 to 1998.